RASĀYAN *J. Chem.*
Vol. 19 | No. 3 | 1883-1889 | July-September | 2026
ISSN: 0974-1496 | e-ISSN: 0976-0083 | CODEN: RJCABP
http://www.rasayanjournal.com
http://www.rasayanjournal.co.in

CANDLENUT SHELL-DERIVED CARBON DOTS AS A POTENTIAL NANOCARRIER OF AMLODIPINE BESYLATE

Riska[1], S. Gea[2], Y. A. Lubis[1], S. Nurafifa[2], and Marpongahtun[2,✉]

[1]Postgraduate School, Department of Chemistry, Faculty of Mathematics and Natural Sciences, Universitas Sumatera Utara, Medan, 20155, Indonesia

[2]Department of Chemistry, Faculty of Mathematics and Natural Sciences, Universitas Sumatera Utara, Medan, 20155, Indonesia

✉Corresponding author: marpongahtun@usu.ac.id

ABSTRACT

Candlenut shell–derived carbon dots (CS-CDs) and nitrogen-doped carbon dots (CS-NCDs) were successfully synthesised via the hydrothermal method, exhibiting blue fluorescence emission and successful conjugation with amlodipine besylate (AB). Photoluminescence (PL) characterisation revealed emission peaks at 498 nm for CS-CDs and 501 nm for CS-NCDs, with corresponding quantum yield (QY) of 25.55% and 20.08%, respectively. HR-TEM and XRD analyses confirmed that the synthesised particles were spherical, semi-crystalline, and possessed sizes below 10 nm. The AB@CS-NCDs conjugate exhibited a higher drug loading capacity (DLC) of 59.21%, with a slightly lower drug loading efficiency (DLE) of 98.58%, whereas CS-CDs showed DLC of 46.05% and DLE of 98.90%. Despite the marginal decrease in DLE observed for CS-NCDs and the lower DLC for CS-CDs, both systems maintained exceptionally high drug loading efficiencies. The significantly enhanced DLC of CS-NCDs indicates that nitrogen-containing functional groups play a dominant role in strengthening drug nanocarrier interactions. These results demonstrate that CS-CDs and CS-NCDs are capable of efficiently accommodating AB within a hydrophilic nanocarrier matrix, thereby suggesting a promising nanomaterial-based drug delivery system (DDS) approach to address the limited aqueous solubility of AB.

Keywords: Carbon Dots, Amlodipine Besylate, Quantum Yield, Drug Loading Efficiency, Drug Loading Capacity.

INTRODUCTION

Amlodipine besylate (AB) is a widely used dihydropyridine calcium channel blocker with proven efficacy in hypertension therapy.[1] However, its low aqueous solubility limits conventional formulation and drug delivery performance, necessitating alternative delivery strategies to support *SDG-3: Good Health and Well-Being*. Carbon dots (CDs) have emerged as promising nanocarriers due to their excellent water solubility, biocompatibility, dispersibility, high surface area, and π-conjugated carbon core enriched with hydrophilic functional groups.[2] CDs, first reported in 2004, possess zero-dimensional structures with particle sizes below 10 nm and exhibit favourable optical properties, including efficient two-photon excitation.[3,4] These attributes render carbon dots highly attractive as nanocarriers for a drug delivery system (DDS).[5] Candlenut shell (*Aleurites moluccana*) is an abundant and sustainable biomass source for CS-NCDs synthesis.[6] Nitrogen heteroatom doping further enhances the optical properties and functional versatility of CS-NCDs for biomedical applications.[7] In this study, CS-NCDs were synthesised via a hydrothermal method due to their simplicity, cost-effectiveness, and environmental compatibility. The resulting CS-NCDs contain abundant −OH, −COOH, and $-NH_2$ surface groups, which facilitate improved drug loading performance in drug delivery systems.[4] In this study, synthesised CS-NCDs were conjugated with AB, and their performance was comparatively evaluated. Nitrogen incorporation into the carbon framework has been reported to enhance the aqueous interaction and bioavailability of AB.[6] Owing to their small size and ease of conjugation, CS-CDs are attractive nanocarriers; however, systematic studies on their ability to accommodate poorly water-soluble drugs such as AB remain limited. Therefore, this work investigates CS-CDs with tailored surface functionality as nanocarriers and evaluates their drug loading performance, providing insights into formulation suitability for overcoming the low aqueous solubility of amlodipine besylate.

http://doi.org/10.31788/RJC.2026.1939744

EXPERIMENTAL

Materials

The candlenut shells (CS) were collected from a plantation in Muara Tembesi, Jambi, Indonesia. Urea (Merck), distilled water, and phosphate-buffered saline (PBS, pH 7.4) were purchased from CV. Rudang Jaya, Medan, Indonesia. Deionised water (PUREAQUA; TOC < 10 ppb, conductivity 0.055 µS/cm at 25 °C, and resistivity 18.2 MΩ·cm) was supplied by PT. PRINCO, Indonesia. Amlodipine besylate (AB) tablets (10 mg) were obtained from PT. Hexpharm, Indonesia. All reagents were used without further purification.

Preparation of CS and Synthesis of CS-CDs, and CS-NCDs

CS was washed with deionised water, sun-dried for 3 days, and carbonised at 300 °C for 6h. Subsequently, 10 g of carbonised powder was dispersed in 50 mL of deionised water and subjected to hydrothermal treatment at 220 °C for 8 h. The resulting suspension was ultrasonicated, centrifuged at 5000 rpm for 30 min, and filtered using Whatman No. 42 paper to obtain CS-CDs. For CS-NCDs synthesis, 1 g of urea was incorporated prior to hydrothermal treatment. The overall synthesis pathway is illustrated schematically in Fig.-1.

Fig.-1: Schematic Representation of (a) the Carbonisation of CS, (b) the Fabrication of CS-CDs, and (c) the Preparation of CS-NCDs via the Hydrothermal Synthesis

Conjugation of AB with Carbon Dots and Drug Loading Determination

For the preparation of AB–conjugated CS-NCDs (AB@CS-NCDs), the AB@CS-NCDs system was synthesised following the procedure described in the reference by Dada.[8] Briefly, 8 mg/mL of the CS-NCDs solution was transferred into a 50 mL volumetric flask, followed by the addition of 4 mg/mL AB solution. The mixture was then diluted to the calibration mark using phosphate-buffered saline (PBS, pH 7.4) and homogenised thoroughly. The resulting AB@CS-NCDs dispersion was stored at 4 °C prior to further experimentation. The same procedure was repeated using CS-CDs to obtain the AB@CS-CDs conjugate. Then, the drug loading capacity (DLC) and drug loading efficiency (DLE) were calculated according to the method reported by Dada.[8] The concentration of unbound AB was quantified using a standard AB calibration curve (linear regression equation) after measuring the absorbance of free AB within the 200–400 nm wavelength range. The amount of AB conjugated to the CS-CDs and CS-NCDs was determined by subtracting the concentration of free AB from the initial concentration of AB. X is classified as CS-CDs or CS-NCDs. The DLC and DLE values were calculated using Equations (1) and (2), respectively, as follows:

$$DLC\ (mg/g) = \frac{AB - Amount\ of\ AB\ contained\ in\ X}{Initial\ number\ of\ X} \quad (1)$$

$$DLE\ (\%) = \frac{Amount\ of\ AB\ contained\ in\ X}{AB}\ x100\% \quad (2)$$

Quantum Yield Determination

The quantum yield (QY) of CS-CDs and CS-NCDs was calculated using quinine sulfate (QS) as a reference standard, following Equation (3)[9]:

$$QY_c = QY_h \times \frac{Ic}{Ih} \times \frac{Ac}{Ah} \times \left(\frac{\eta c}{\eta h}\right)^2 \quad (3)$$

QS, with a reported quantum yield of 54% and a refractive index of 1.33, was employed to determine the relative fluorescence efficiency of the synthesised carbon dots. In this calculation, the quantum yield is derived from the ratio of the integrated photoluminescence emission intensity and absorbance of the samples relative to the reference, while also accounting for differences in the refractive index of the solvents. The subscripts "c" and "h" denote the CS-CDs or CS-NCDs samples and the QS reference, respectively.

RESULTS AND DISCUSSION

Structural and Crystallographic Characteristics

The structural and crystallographic characteristics were further examined using HR-TEM, as presented in Fig.-2(a–d). The obtained images show average particle sizes of approximately 0.60 nm for CS-CDs and 1.79 nm for CS-NCDs, which are consistent with previous reports and correspond to the (003) plane of graphitic carbon. As shown in Fig.-2(d), the Raman spectra confirm a satisfactory degree of graphitisation in both CS-CDs and CS-NCDs. The spectra exhibit characteristic D (1387 cm^{-1}) and G (1593 cm^{-1}) bands for CS-CDs, and D (1370 cm^{-1}) and G (1587 cm^{-1}) bands for CS-NCDs, representing vibrational modes of sp^2-hybridised carbon atoms arranged in aromatic domains. The calculated I_D/I_G ratios were 0.863 for CS-CDs and 0.871 for CS-NCDs, indicating the presence of structural disorder, surface defects, vacancies, and possible heteroatom incorporation such as nitrogen doping.[10] Additionally, the HR-TEM micrographs (Fig.-2a–b) reveal that both samples exhibit quasi-spherical morphology with uniform particle distribution.[11]

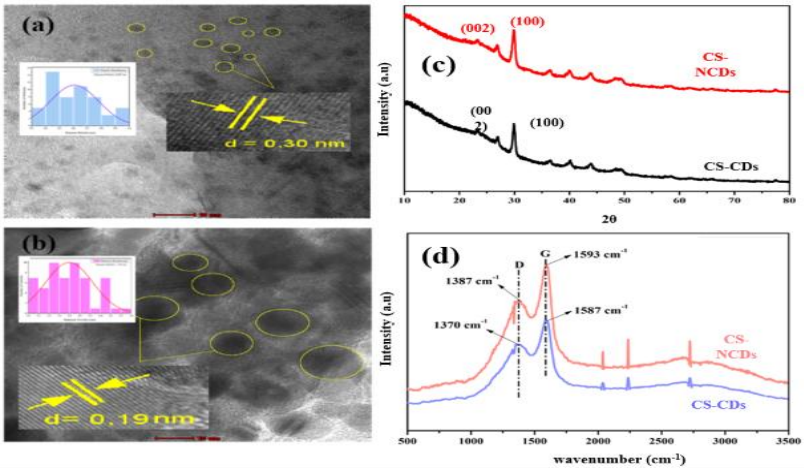

Fig.-2: HR-TEM Images with Lattice Fringes and Inset Particle Size Histograms (a–b); XRD Patterns (c); and Raman Spectra (d) of CS-CDs and CS-NCDs

In the HR-TEM images in Fig.-2(a–b), the CS-NCDs exhibit a larger particle size compared to the CS-CDs, and both samples demonstrate characteristics of a semi-crystalline structure. The lattice fringes show interlayer spacings of approximately 0.30 nm for CS-CDs and 0.19 nm for CS-NCDs, corresponding to the graphite structure.[12] The increase in particle size is attributed to the introduction of a nitrogen source during synthesis, which alters the nucleation process and growth kinetics of the CDs. The structural characteristics are further confirmed by the XRD patterns, indicating that both samples possess semi-crystalline features, as shown in Fig.-2(c). Diffraction peaks corresponding to the (002) and (100) crystal planes are observed, with broad yet slightly intensified peaks appearing at approximately $2\theta \approx 24°$ (002) and 30° (100). The broadening of these peaks is attributed to the partially amorphous nature of the carbon matrix.[13]

Characterization by FTIR, XPS, and Optical Properties

The FTIR spectra in Fig.-3(a–b) reveal the functional groups of the CS precursor, CS-CDs, and CS-NCDs. The CS sample exhibits absorption peaks at 3183 cm^{-1} (C–H stretching), 2102 cm^{-1} and 1580 cm^{-1}(C=C stretching), 1908 cm^{-1} (C=O stretching), and ~1200 cm^{-1} (C–O). Additional bands at 1416, 872, 755, and 685 cm^{-1} correspond to C–H deformation vibrations. These spectral features indicate a carbon-rich precursor suitable for CS-CDs and CS-NCDs synthesis.

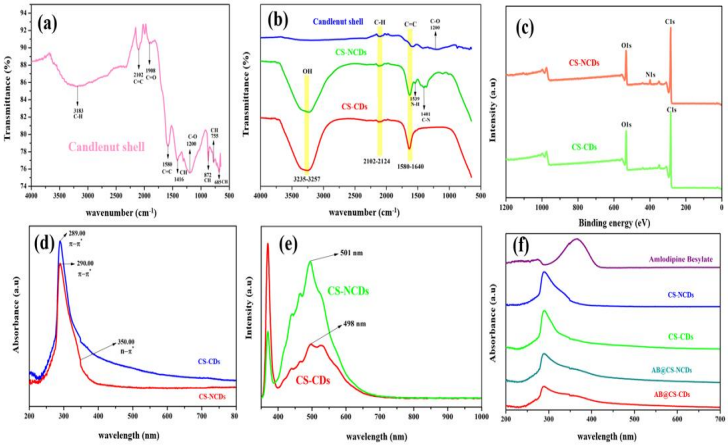

Fig.-3: FTIR (a) CS, (b) CS-CDs, CS-NCDs, and CS, Binding Energy of (c) CS-CDs and CS-NCDs, Spectrum UV-Vis (d) CS-CDs and CS-NCDs, FL Spectra (e) CS-CDs and CS-NCDs, and UV Vis (f) Amlodipine Besylate, CS-NCDs, CS-CDs, AB@CS-NCDs, and AB@CS-CDs

The FTIR spectra of the synthesised CS-CDs and CS-NCDs reveal the presence of hydrophilic and biocompatible functional groups. Both CS-CDs and CS-NCDs display broad absorption bands at 3253–3257 cm^{-1}, which is characteristic of O–H stretching vibrations, implying that hydroxyl groups are present on the material surface.[14] Peaks in the range of 2102–2124 cm^{-1} correspond to C–H stretching, whereas characteristic C=C stretching is detected between 1580–1640 cm^{-1}. The presence of C=C and C–O functionalities supports the formation of a graphite-like carbon framework, consistent with the structural evidence obtained from HR-TEM and Raman spectroscopy.[7] Distinct functional features associated with nitrogen doping are observed in CS-NCDs, where peaks at 1539 cm^{-1} and 1401 cm^{-1} indicate contributions from N–H and C–N bonds, respectively.[15] The abundance of oxygen and nitrogen-bearing surface functionalities, including hydroxyl (O–H), carbonyl (C=O), and C–N groups, contributes to the high dispersibility and aqueous stability of both carbon dot samples.[7] These results confirm the presence of hydroxyl and alkyl groups on the CD surface, which further enhance their colloidal stability and interaction potential.[16] The electronic transitions associated with these functional groups are corroborated by the UV–Vis spectra shown in Fig.-3(d). Both samples exhibit strong absorption peaks at 289 nm (CS-CDs) and 290 nm (CS-NCDs), corresponding to π–π* transitions of C=C bonds and n–π* transitions associated with C=O and C–N groups, particularly in the nitrogen-doped structure.[17] The FTIR and UV–Vis results are further corroborated by the XPS spectra shown in Fig.-3(c). The high-resolution C1S spectra of CS-CDs and CS-NCDs exhibit peaks at 284.69 eV and 284.72 eV, respectively, corresponding to C–C/C=C bonds from graphitic and sp^3-hybridized carbon. The O1S peaks at 531.69 eV (CS-CDs) and 531.72 eV (CS-NCDs) confirm the presence of carbonyl (C=O) groups, while the N1S signals at 399.69 eV and 398.72 eV are attributed to pyridinic C–N bonding. These findings indicate that hydroxyl and epoxide groups dominate the surface chemistry, with limited nitrogen incorporation into the sp^2 carbon framework (1.58% for CS-CDs and 5.44% for CS-NCDs). This result is consistent with XRD patterns showing reflection peaks at 2θ≈24° (002) and 30° (100), indicating enhanced graphitic crystallinity. Fluorescence spectra in Fig.-3(e) further support these observations, where red-shifted emission correlates with increased graphitic nitrogen and reduced pyridinic nitrogen content.[18] UV–Vis spectra in Fig.-3(f) reveal clear spectral shifts after conjugation with AB. The addition of CS-CDs (8 mg/mL) induces a shift from 289 nm to 293 nm for both AB@CS-CDs and AB@CS-NCDs, along with bathochromic shifts at

367 nm and 370 nm compared to free AB (367 nm), indicating successful interaction between AB and the carbon dots. FTIR analysis in Fig.-4(a–b) further confirms AB attachment. While free AB shows characteristic C=O, N–H, and C=C vibrations, AB@CS-CDs and AB@CS-NCDs display new absorption bands at 2841 cm^{-1} and 2918 cm^{-1}(aromatic C–H stretching) and deformation bands at 1009–1081 cm^{-1}, confirming conjugation.

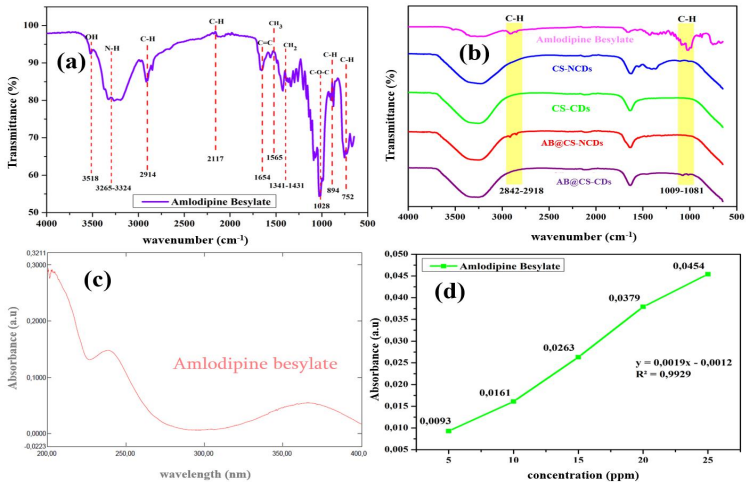

Fig.-4: FTIR (a) AB, (b) Amlodipine Besylate, CS-NCDs, CS-CDs, AB@CS-NCDs, AB@CS-CDs, Spectrum UV-Vis (c) AB, Calibration Curve of (d) AB

Additional verification is provided by UV–Vis spectroscopy (Fig.-4(c)), where AB exhibits a λmax at 238 nm with an absorbance of 0.1479, consistent with reported values (236–238 nm). The calibration curve in Fig.-4(d) shows a linear regression of y=0.0019x−0.0012 with R^2=0.9929 (R=0.9929), demonstrating excellent linearity and analytical reliability.[19]

Drug Loading Performance

To evaluate the drug loading performance, the DLC and DLE were calculated. These values were determined based on UV–Vis absorbance measurements at a wavelength of 238 nm. The DLC and DLE percentages were determined based on Equations (1) and (2), and the calculated results are presented in Table-1.

Table-1: Results of DLC and DLE.

Sample	DLC (%)	DLE (%)	References
AB	20.00	42.00	20
AB@CS-CDs	46.05	98.90	This work
AB@CS-NCDs	59.21	98.58	This work

The DLC value of AB@CS-NCDs (59.21%) is higher than that of AB@CS-CDs (46.05%), indicating a greater drug loading capacity due to the increased density of active binding sites introduced by nitrogen doping. In contrast, AB@CS-CDs exhibit a slightly higher DLE (98.90%) compared to AB@CS-NCDs (98.58%), reflecting a more efficient drug loading process in which a larger fraction of the initial drug is successfully bound. These results confirm successful drug loading for both systems.

As shown in Fig.-5, the observed differences in DLC and DLE are governed by the surface properties of the nanocarriers: CS-CDs show high loading efficiency but limited capacity, whereas nitrogen-doped CS-NCDs provide a higher density of active sites, including –C=N– bonds, enabling greater drug accommodation with a marginal decrease in efficiency.[21] These findings highlight the important role of nitrogen-containing surface functionalities in modulating drug loading behaviour and provide additional insight into the structure–property relationship of carbon dot–based nanocarriers for poorly water-soluble drugs such as amlodipine besylate.

CONCLUSION

CS-CDs and CS-NCDs derived from CS biomass were successfully characterised to assess the effect of nitrogen incorporation. Both nanocarriers were effectively conjugated with amlodipine besylate,

exhibiting initial DLC and DLE values of approximately 20% and 40%, respectively. After conjugation, AB@CS-CDs showed DLC and DLE values of 46.05% and 98.90%, while AB@CS-NCDs exhibited a higher DLC (59.21%) with a slightly lower DLE (98.58%).

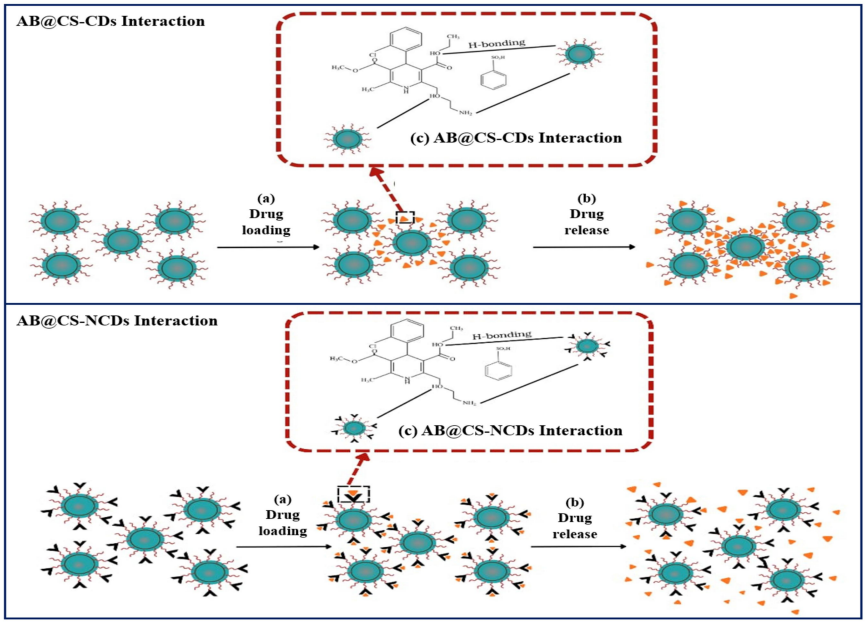

Fig.-5: Schematic Illustration of AB Loading/Release in CS-CDs and CS-NCDs, Including Hydrogen Bonding Interactions Between AB And Nanocarrier Surface Groups

These findings demonstrate that nitrogen-assisted surface engineering enables the tuning of DLC and DLE for poorly soluble drugs such as amlodipine besylate, thereby supporting *SDG-3: Good Health and Well-Being*, through the development of more efficient drug delivery systems to improve therapeutic effectiveness and healthcare outcomes.

ACKNOWLEDGMENTS

The authors gratefully acknowledge the Ministry of Education, Culture, Research, and Technology of Indonesia for financial support through the PTM research grant no. 78/UN5.3.2.1/PPM/KP-DRTPM/B/2023.

CONFLICT OF INTERESTS

The authors declare that there is no conflict of interest.

AUTHOR CONTRIBUTIONS

The present work is related to *SDG-3: Good Health and Well-Being*. All the authors contributed significantly to this manuscript, participated in reviewing/editing and approved the final draft for publication. The research profile of the authors can be verified from their ORCID ids, given below:

Riska https://orcid.org/0009-0007-2251-2663
Saharman Gea https://orcid.org/0000-0003-0615-0918
Yuni Aldriani Lubis https://orcid.org/0009-0009-1494-6861
Siti Nurafifa https://orcid.org/0009-0007-8497-1216
Marpongahtun https://orcid.org/0000-0003-1050-0431

Cite this article as: Riska *et al.*, *Rasayan J. Chem.*, 19(3), 1883-1889(2026), https://doi.org/10.31788/RJC.2026.1939744

REFERENCES

1. J. L. Morgan, B. K. Kogutt, C. Meek, E. K. Stehel, D. D. McIntire, J. S. Sheffield and S. W. Roberts, *Pregnancy Hypertension*, **11**, 77(2018), https://doi.org/10.1016/J.PREGHY.2018.01.002
2. F. Maleki, N. Hadidi and M. Parandin, *Journal of Luminescence*, **291**, 121695(2026), https://doi.org/10.1016/J.JLUMIN.2025.121695
3. M. A. González-Reyna, G. A. Molina, K. Juarez-Moreno, A. Rodríguez-Torres, R. Esparza, and M. Estevez, M, *Biomaterials Advances*, **153**, 213561(2023), https://doi.org/10.1016/J.BIOADV.2023.213561
4. Marpongahtun, Andriayani, Y. Muis, S. Gea, S. A. Amaturrahim, B. Attaurrazaq and A. Daulay, *International Journal of Technology*, **14(1)**, 219(2023). https://doi.org/10.14716/ijtech.v14i1.4863
5. M. González and M. P. Romero, *International Journal of Nanomedicine*, **20**, 7715(2025), https://doi.org/10.2147/IJN.S508181
6. K. Kirubanithy and A. Santhanam, *Scientific Reports*, **15(1)**, 33885(2025), https://doi.org/10.1038/s41598-025-06307-z
7. Y. Aldriani Lubis, S. Gea, M. Frassetia Lubis and W. Wu Larry Pai, *Indonesian Journal of Chemical Research*, **13(1)**, 38(2025), https://doi.org/10.30598//ijcr.2025.13-yun
8. S. N. Dada, G. K. Babanyinah, M. T. Tetteh, V. E. Palau, Z. F. Walls, K. Krishnan, Z. Croft, A. U. Khan, G. Liu, T. E. Wiese, E. Glotser and H. Mei, H, *ACS Omega*, **7(27)**, 23322(2022), https://doi.org/10.1021/acsomega.2c01482
9. A. V. Longo, A. Sciortino, M. Cannas and F. Messina, F, *Physical Chemistry Chemical Physics*, **22(24)**, 13398(2020), https://doi.org/10.1039/d0cp00952k
10. S. Kariminia, M. Shamsipur and A. Barati, *International Journal of Biological Macromolecules*, **254**, 127728(2024), https://doi.org/10.1016/J.IJBIOMAC.2023.127728
11. J. Anum, M. A. Akhtar, A. M. Khan, K. Ahmed, C. M. Sayes, A. M. Almajwal, J. Iqbal and A. Rahim, *Journal of Water Process Engineering*, **77**, 108472(2025), https://doi.org/10.1016/J.JWPE.2025.108472
12. H. Ghahremani, M. J. Molaei and E. Salimi, E, *Diamond and Related Materials*, **158**, 112615(2025), https://doi.org/10.1016/J.DIAMOND.2025.112615
13. H. Ferjani, S. Abdalla, O. A. Oyewo and D. C. Onwudiwe, D. C, *Inorganic Chemistry Communications*, **160**, 111866(2024), https://doi.org/10.1016/J.INOCHE.2023.111866
14. K. I. Magowe, P. Dinake and L. Lebogang, *Results in Chemistry*, **16**, 102412(2025), https://doi.org/10.1016/J.RECHEM.2025.102412
15. H. Yorozuya, N. E. Ashrafi, K. Sato, A. Islam, R. Fukae, Y. Tagashira and T. Limori, *Molecules*, **30(9)**, 2068(2025), https://doi.org/10.3390/molecules30092068
16. D. Soren, J. Panda, J. Swain, A. Priyadarshini, S. Swain, J. Swain, R. Pati, S. R. Mohapatra, Y. Das, R. Samantaray and R. Sahu, *Scientific Reports*, **15(1)**, 33727(2025), https://doi.org/10.1038/s41598-025-87341-9
17. Y. Xu, Y. Hao, M. Arif, X. Xing, X. Deng, D. Wang, Y. Meng, S. Wang, M. S. Hasanin, W. Wang and Q. Zhou, *International Journal of Nanomedicine*, **19**, 5879(2024), https://doi.org/10.2147/IJN.S453385
18. J. Jia, X. Liu and W. Wang, W, *Nanomaterials*, **15(13)**, 976(2025), https://doi.org/10.3390/nano15130976
19. A. Rai and S. Sharma, *Asian Journal of Pharmaceutical Research and Development*, **7(5)**, 42(2019), https://doi.org/10.22270/ajprd.v7i5.560
20. A. Arora, N. Shafiq, S. Jain, G. K. Khuller, S. Sharma and S. Malhotra, *PLoS ONE*, **10(6)**, e0128208 (2015), https://doi.org/10.1371/journal.pone.0128208
21. A. Hussain, M. F. Alajmi and S. Ganguly, *Diamond and Related Materials*, **145**, 111101(2024), https://doi.org/10.1016/J.DIAMOND.2024.111101

[RJC-9744/2026]